Silicon-Vacancy Nanodiamonds as High Performance Near-Infrared Emitters for Live-Cell Dual-Color Imaging and Thermometry

Weina Liu†∇⁺°, Md Noor A Alam†∇°, Yan Liu§, Viatcheslav N. Agafonov⊥, Haoyuan Qi‖‡, Kaloian Koynov†, Valery A. Davydov#, Rustem Uzbekov○+, Ute Kaiser‖, Theo Lasser†, Fedor Jelezko§, Anna Ermakova†⊥* and Tanja Weil†∇**

†Max-Planck-Institute for Polymer Research, Ackermannweg 10, 55128 Mainz, Germany

∇Institute of Inorganic Chemistry I, Ulm University, Albert-Einstein-Allee 11, 89081 Ulm, Germany

†Institute of Materials, École Polytechnique Fédérale de Lausanne, Station 12, 1015 Lausanne, Switzerland

§Institute for Quantum Optics, Ulm University, Albert-Einstein-Allee 11, 89081 Ulm, Germany

⊥GREMAN, UMR CNRS-7347, Université de Tours, 37200, Tours, France

‖Central Facility for Electron Microscopy, Ulm University, Albert-Einstein-Allee 11, 89081 Ulm, Germany

‡Center for Advancing Electronics Dresden (cfaed) and Food Chemistry, Technical University of Dresden, 01069 Dresden, Germany

#L.F. Vereshchagin Institute for High Pressure Physics, The Russian Academy of Sciences, Troitsk, Moscow, 108840, Russia

○Laboratoire Biologie Cellulaire et Microscopie Electronique, Faculté de Médecine, Université François Rabelais, 37032 Tours, France

+Faculty of Bioengineering and Bioinformatics, Moscow State University, 119992, Leninskye gory 73, Moscow, Russia

⏚ Institute for Physics, Johannes Gutenberg University Mainz, Staudingerweg 7, 55128 Mainz, Germany

° Contributed equally

* Corresponding authors

KEYWORDS. Nanodiamond, silicon vacancy color center, near infrared cellular imaging, live cell particle tracking.

ABSTRACT. Nanodiamonds (NDs) with color centers are excellent emitters for various bioimaging and quantum biosensing applications. In our work, we explored new applications of NDs with silicon-vacancy centers (SiV) obtained by high-pressure high-temperature (HPHT) synthesis based on metal-catalyst-free growth. They are coated with a polypeptide biopolymer which is essential for efficient cellular uptake. The unique optical properties of NDs with SiV are their high photostability and narrow emission in the near-infrared region. Our results demonstrate

for the first time that NDs with SiV allow live-cell dual-color imaging and intracellular tracking. Also, intracellular thermometry as well as challenges associated with SiV atomic defects in NDs are investigated and discussed for the first time. NDs with SiV nanoemitters provide new avenues for live-cell bioimaging, diagnostic (SiV as a nanosized thermometer), and theranostic (nanodiamonds as drug carrier) applications.

Currently, fluorescent molecules are mostly used as labels for intracellular imaging. However, their applications are limited by a fast-photobleaching time, which makes them ineffective for time-laps monitoring. A promising alternative are nanodiamonds (NDs) with color centers that demonstrate high photostability.[1] Depending on the type of color center they can be used for bioimaging and sensing applications, such as super-resolution imaging and nanoscale magnetic field, and temperature sensing.[2-4] The most investigated diamond color center is the nitrogen-vacancy center (NV), which consists of a substitutional nitrogen atom next to a carbon vacancy. NDs with NV (ND-NV) are commercially available and can be produced in different sizes and with varying numbers of NVs.[5] The NV center reveals two charge states: the neutral NV^0 or the negative NV^- state that both have stable fluorescence, but only the NV^- state is suitable for quantum sensing application.[6] Zero phonon lines (ZPL) of NV^0 and NV^- are accompanied by broad phonon sidebands, leading to broad fluorescence emission spanning from ~575 nm (NV^0) or 637 nm (NV^-) to 800 nm.[6] Although ND-NV can be used for long-term bioimaging studies, their fluorescence spectrum partly overlaps with many other optical markers as well as the background emission of cells so that dual/multicolor imaging remains challenging. In contrast, NDs with negatively charged silicon-vacancy centers (SiV) have recently received considerable attention as potential high-performance bioimaging probes due to their attractive optical properties with sharp emission in the near-infrared (NIR) range.[7] In the diamond lattice, the silicon atom

with its larger size compared to the carbon atom replaces two carbon atoms and is located between these two vacancies (Figure 1a). This divacancy structure of the center has inversion symmetry resulting in low sensitivity to strain and contributes to a narrowing of the optical emission.[7] Due to the low electron-phonon coupling, more than 70% of the SiV emission is dominated by the sharp ZPL at ~738 nm with the full width at half maximum (FWHM) of approximately 4 nm.[7] The NIR emission of ND-SiV allows deeper tissue penetration and *in vivo* optical imaging.[8,9] Moreover, the ZPL peak position of SiV has a temperature signature, which is linearly correlated to temperature changes in the range of 295 ± 5 K with sub-kelvin sensitivity.[10] The combination of NIR emission, narrow bandwidth, high photo- and chemical stability, and temperature-dependent ZPL[11,–12] renders ND-SiV as promising candidates for bioimaging and temperature sensing applications in life sciences.

In this work, we report the production and functionalization of ND-SiV for live-cell dual-color imaging, thermometry, and tracking. We optimized the metal-catalyst-free high-pressure high-temperature (HPHT) approach to synthesize ND-SiV with radii of about 50 nm and without the presence of NV centers. The ND-SiV surface was coated by a protein-derived biopolymer based on multiple electrostatic interactions resulting in nanoparticles with enhanced colloidal stability. These coated ND-SiV reveal a good uptake by HeLa and A549 cells based on an endocytosis mechanism. For the first time, HPHT ND-SiV were used for live-cell dual-color imaging based on their NIR emission, high photostability, and sharp ZPL. Moreover, the first intracellular thermometry by ND-SiV with radii 50 nm and less was demonstrated.

Traditionally NDs are synthesized by HPHT growth in the presence of transition metal catalysts or chemical vapor deposition (CVD) growth.[13] The color centers can be introduced by adding impurities during diamond growth or by ion implantation. The metal-catalyst-free synthesis is

more preferable for fluorescent NDs production since metal atoms can introduce additional defects into the crystal structure, which can deteriorate the properties of the color centers. Such a method is based on the conversion of organic and heteroorganic solids into diamond.[14,15] This technique allows controlling ND sizes as well as the concentration of the color centers.[16,17] Herein, we present the production of ND-SiV from a homogeneous mixture of naphthalene ($C_{10}H_8$, Chemapol), octafluoronaphthalene ($C_{10}F_8$, Alfa Aesar), detonation NDs (3-4 nm, SkySpring), and tetrakis(trimethylsilyl)silane ($C_{12}H_{36}Si_5$, Stream Chemicals Co.), which was used as the doping component (Figure 1b). The introduction of fluorine-containing compounds into the growth system leads to the reduction of the content of NV in NDs.[15,16,18] Detonation NDs were introduced into the growth medium as seeds in the HPHT reaction to obtain higher yields. This carbon and silicon source mixture was cold-pressed as a tablet (5 mm diameter and 4 mm height) and placed into a graphite container, which simultaneously served as a heater for the high-pressure Toroid-type apparatus. The HPHT growth comprised the following steps: (1) reaching high pressure (8.0 GPa) at room temperature, (2) heating to high temperature (~1400 °C) for diamond formation, and (3) an isothermal exposure for short time (3 s). Then the temperature decreased to room temperature, while the pressure remained high. The applied conditions triggered NDs formation inside the initial tablet of the pressed components. Five batches were synthesized under the same conditions and combined to maximize the amount of ND powder. Steel ball milling was applied to break the obtained tablets into micro- and nanoparticles before chemical cleaning. A primary cleaning step with HNO_3:$HClO_4$:H_2SO_4 at 230 °C for 5 h generated a powder, which was then neutralized with NH_4OH buffer, washed, and dried as depicted in Scheme S1.

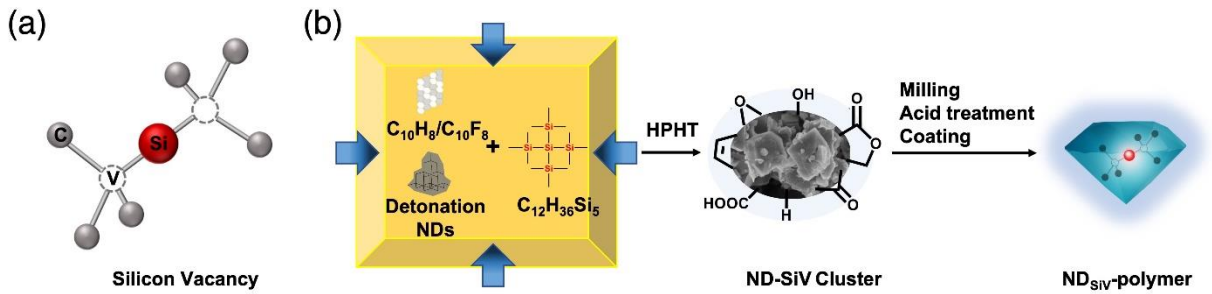

Figure 1. (a) The atomic structure of SiV center is displayed by one silicon atom (Si) with two adjacent atom vacancies (V) in the diamond lattice of carbon atoms (C). (b) Schematic presentation of ND-SiV HPHT synthesis and modification by coating.

Scanning and transmission electron microscopy (SEM and TEM, Figure S1 and S2) showed the formation of diamonds of nano- and micrometer sizes with cuboctahedral shapes. The photoluminescence (PL) measurements revealed the very sharp SiV spectrum (Figure 2e), without the presence of NV due to the application of $C_{10}F_8$ as a starting material during synthesis. In contrast, NDs synthesized without $C_{10}F_8$ showed strong NV and SiV emissions in their PL spectra (Figure S3). The demonstrated HPHT ND-SiV synthesis offers several distinct advantages: (1) no metal catalyst is employed that could remain as impurities in the NDs, (2) no post-processing by irradiation or annealing is required to activate the color centers, and (3) the method is scalable up to several milligram quantities, which would allow extensive cell studies with high reproducibility in the same batch.

Surface cleaning and oxidization was accomplished by combining acid treatment (HNO_3-H_2SO_4-$HClO_4$, ratio 1:1:1, at 90 °C for 8 h) and sonication (Scheme S1). We obtained about 5 mg of a stable ND-SiV suspension in water without clusters with polar carboxylic acid surface groups [19] allowing further chemical modifications.[20] The dimensions of fluorescent ND-SiV in water

were determined by fluorescence correlation spectroscopy (FCS)[21] and dynamic light scattering measurement (DLS). Nanoparticles with average hydrodynamic radii of 62 ± 5 nm (FCS, Figure 2f) and 52.3 ± 3.6 nm (DLS, Figure 2g) with a polydispersity index (PDI) of 0.16 (Figure S7) were recorded as single nanoparticles (according to FCS) and no ND clusters were observed. Noteworthy, the FCS method detects only fluorescent nanoparticles, whereas DLS determines all NDs in the sample, which could be a reason for the small differences in ND sizes measured by FCS and DLS methods. Besides, there is a difference in the polydispersity averaging index of FCS and DLS measurements.[22] After the acid treatment, the ND-SiV exhibited negative zeta-potential with a single peak distribution (ζ = -29.33 mV, Figure 2h and S8-S10).

The application of ND-SiV for cellular studies requires surface coating that imparts colloidal stability in cell media and allows cellular uptake and trafficking to cellular compartments with low cellular toxicity. We have previously reported the conversion of plasma proteins into biocompatible ND surface coatings that have been applied *in vitro* and *in vivo*.[23] Herein, the abundant serum protein human serum albumin (HSA) was chemically modified by reacting ethylenediamine groups with the carboxylic acid surface groups of aspartic acid and glutamic acid residues yielding cationic HSA (cHSA, cationazation) as described previously and as depicted in Figure S4.[23-25] cHSA with multiple additional amino groups provides multiple positive net charges, which are required for the subsequent formation of stable complexes with a negatively charged surface of ND-SiV by electrostatic interactions. Hydrophilic polyethylene glycol (PEG) chains (average molecular weight of 2000 Da) were conjugated to cHSA to improve the colloidal stability of coated ND-SiV (cHSA-PEO, PEGlytion). Next, the polypeptide backbone of cHSA-PEO was unfolded by the reduction of disulfide bridges. The generated free sulfhydryl groups were capped with *N*-(2-aminoethyl)maleimide to obtain the stable single-chain positively charged

biopolymer (dcHSA-PEO, denaturation). The synthesis and characterization of the biopolymer dcHSA-PEO have been reported previously[23] and are included in the SI (Figure S11 and Figure S12).

ND-SiV were coated with dcHSA-PEO by first diluting the negatively charged nanoparticles in boric acid buffer (0.05 mg mL^{-1}, 20 mL, pH = 8.4) and then titrating the nanodiamond solution into dcHSA-PEO solusion (0.2 mg mL^{-1}, dispersed in the same boric acid buffer, 20 mL). The mixture was stirred overnight and coating proceeded by electrostatic adsorption of the positively charged modified proteins to the nanodiamond surface. After ultrafiltration (cutoff 30 KD) and centrifugation (17000 RPM, 30 min, 3 times), the ND mixture was concentrated, and unbound dcHSA-PEO biopolymer was removed. About 1 mg (50% yield) coated ND-SiV were obtained, termed ND_{SiV}-polymer (Figure 1b). Figure 2a shows the aberration-corrected high-resolution TEM (AC-HRTEM) image of ND_{SiV}-polymer in $[0\bar{1}1]$ projection. Highly crystalline ND_{SiV}-polymer nanoparticles were observed exhibiting sharp edges along the main crystallographic orientations. In the magnified image (Figure 2b), the (111) and (022) lattice planes of diamond were clearly resolved. Residual amounts of amorphous and non-diamond nanoparticles were also observed via AC-HRTEM (Figure S5), which could not be removed by the acid processing. However, the X-ray diffraction patterns (XRD) of the ND-SiV raw material indicated the typical diamond spectrum with reflections at (111) and (220) (Figure S6).

A uniform and discrete distribution of ND_{SiV}-polymer was determined by TEM (Figure 2c), with an average radius of 31.6 nm (histogram in Figure 2d) after analyzing about 108 NDs in the TEM image. After the protein polymer encapsulation, DLS measurements revealed a hydrodynamic radius of ND_{SiV}-polymer in the water of about 63.6 ± 5.3 nm (PDI = 0.1) corresponding to an

increase of about 11 nm due to the protein polymer shell (Figure 2g). The ND_{SiV}-polymer appeared colloidally stable also in phosphate-buffered saline (PBS, pH = 7.4), and the radius increased only slightly to 70 nm (PDI = 0.08, DSL measurements). The surface charges of ND_{SiV}-polymer were positive (ζ = 21.3 mV) due to the presence of the polycationic biopolymer coating dcHSA-PEO. Nanoparticle surface coatings with positive net charges often facilitate cellular uptake due to electrostatic interactions with the negatively charged cellular membranes (Figure 2g and h).[18, 23]

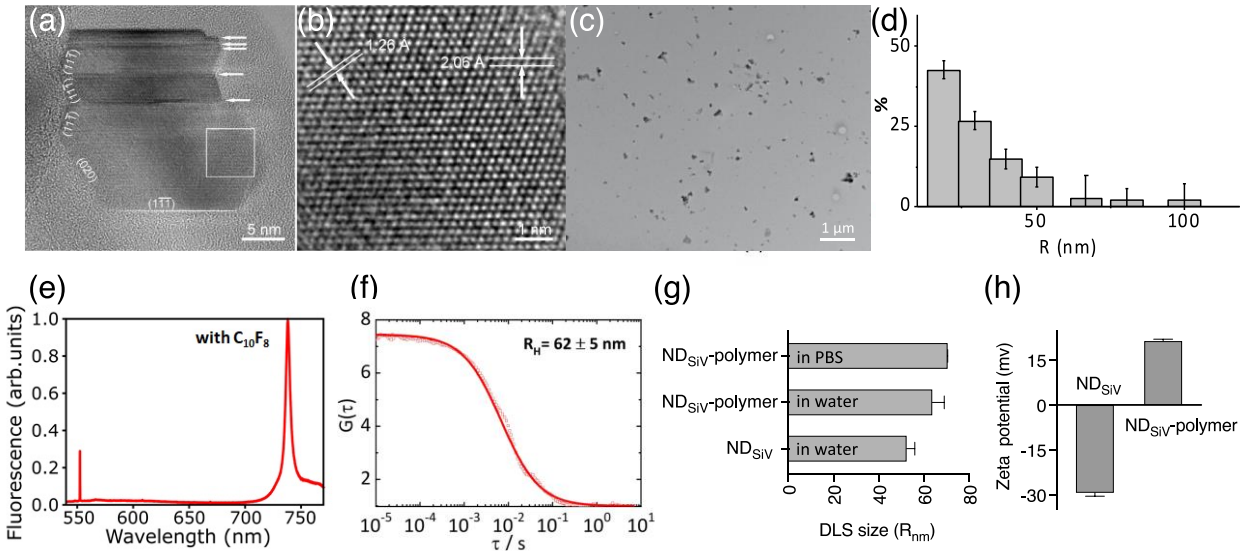

Figure 2. Characterization of ND-SiV and ND_{SiV}-polymer. (a) [0$\bar{1}$1] AC-HRTEM image of ND-SiV consisting of crystalline domains separated by twin boundaries (marked by arrows). (b) Magnified image from the boxed region in (a), showing the distances ***d*** between the diamond lattice planes: (111) (***d***=2.06 Å) and (022) (***d***=1.26 Å). (c) TEM image of coated ND_{SiV}-polymer. Small clusters can be observed from the TEM images, but most of the NDs are discrete nanoparticles. (d) Histogram of NDs radius, quantification of 108 NDs from (c). (e) PL spectra of HPHT ND-SiV synthesized with $C_{10}F_8$. (f) FCS autocorrelation curves of ND-SiV in water solution with the obtained hydrodynamic radii. (g) DLS radius of ND-SiV in water and ND_{SiV}-polymer in water and PBS buffer. (h) Zeta-potential of ND-SiV and ND_{SiV}-polymer.

The ND_{SiV}-polymer was applied for live-cell imaging in HeLa cells used as a model cell line. ND_{SiV}-polymer (0.02 mg mL^{-1}) was incubated for 24 h to enable cellular uptake, which was recorded by confocal laser scanning microscopy (CLSM). In a previous study, ND-SiV powder prepared by the CVD method or by Si implantation was directly added to cells[26] without stabilizing surface modifications. In this case, even after several days of incubation, either limited internalization (NDs prepared by CVD method) or only NDs (prepared by Si implantation) aggregation at the cell surface was observed. In the present study, ND_{SiV}-polymer was taken up and appeared homogeneously distributed within cells (Figure 3a and S13). Due to the high index of refraction, these ND_{SiV}-polymer act as strong light scatterers allowing to distinguish NDs from background fluorescence of HeLa cells, which proved to be very helpful for further multiple stained bioimaging. According to Figure 3a, the images taken in the reflection mode of ND_{SiV}-polymer showed a good localization match with the ND_{SiV}-polymer fluorescence images (colocalization coefficient 0.6), indicating that most NDs contained SiV centers. The non-overlapping portion was attributed to a small fraction of NDs lacking SiV centers since the reflection imaging depicts all ND particles, and fluorescence imaging shows only NDs with color centers. It has been reported that SiV within NDs could blink and bleach by pathways still not fully understood.[27] Furthermore, a time series scan was processed to evaluate the photostability of ND_{SiV}-polymer. Some of the fluorescent points bleached after three scanning sweeps (Figure S14a), but the remaining emitters showed high stability (Figure S14b) making them suitable for cellular imaging and nanoparticle monitoring.

HeLa cells incubated with ND_{SiV}-polymer were placed under a customized scanning confocal microscope for cell imaging (Figure 3b). The cell culture medium was replaced with a phenol red-free buffer to avoid additional fluorescence. Laser excitation at 532 nm with the power of 200 μW

(measured before the objective) was performed and the fluorescence was recorded simultaneously by two different detection channels. Channel 1 with a long-pass filter detected the light with a wavelength longer than 575 nm (Figure 3b, (i, iii)). Channel 2 had a band-pass filter to register emitted light in the range of 720-760 nm corresponding to the SiV fluorescence. The initial images of HeLa cells incubated with ND_{SiV}-polymer are presented in Figure 3b (i, ii). In channel 1 (Figure 3b (i)), we observed SiV together with the autofluorescence of the cell. To prove the presence and position of ND_{SiV}-polymer only, channel 2 was successfully used (Figure 3b (ii)) where autofluorescence of the cell was filtered. Cell autofluorescence was very weak, therefore, the CellMask green dye was added to the sample for better cell visualization (Figure 3b (iii, iv)). The signal from CellMask green was a few orders of magnitude higher than that of SiV due to the high number of dye molecules in the focal spot (Figure 3b (iii)). However, the presence of membrane dyes did not interfere with the imaging of ND_{SiV}-polymer in channel 2 (Figure 3b (iv)). These experiments proved the suitability of ND-SiV for dual-color live-cell imaging because the sharp NIR ZPL emission of ND-SiV could be easily separated from many dyes and drugs.

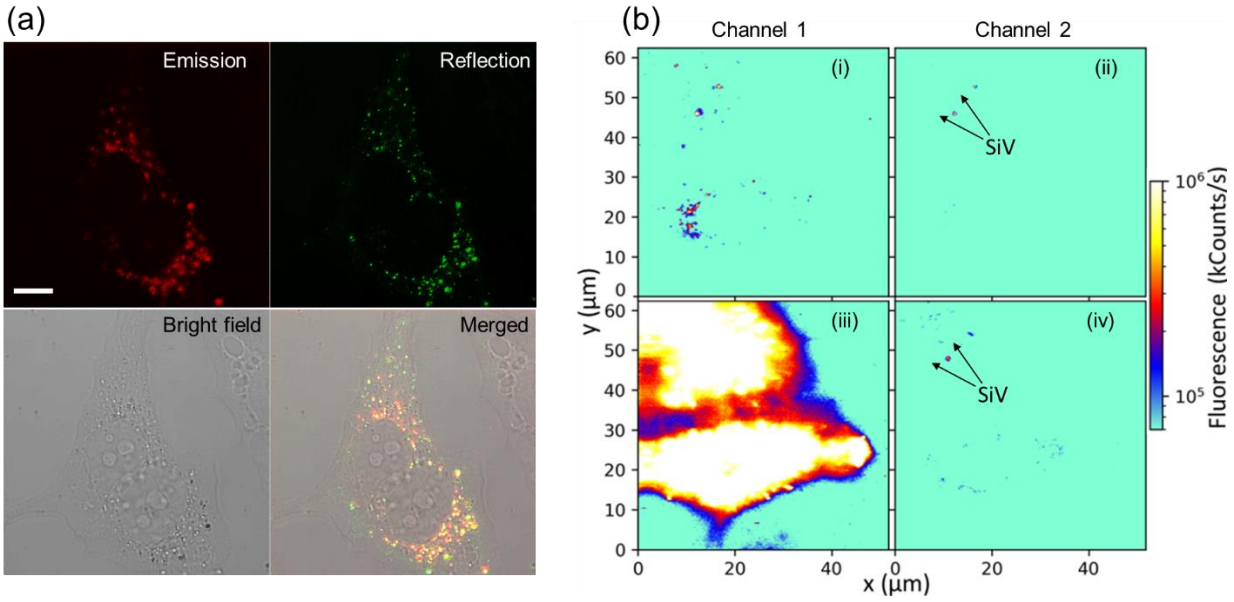

Figure 3. ND_{SiV}-polymer for dual-color cell imaging. (a) CLSM cell images showing efficient cell uptake. Emission and reflection channels demonstrated very good colocolization (λ_{ex} = 561 nm, λ_{em} = 700 – 758 nm, λ_{re} = 556 – 566 nm, scale bar = 10 μm). (b) The fluorescence cell images obtained by a customized scanning confocal microscope (λ_{ex} = 532 nm) with two detection channels (1 – λ_{em} = 575 nm and longer, 2 – λ_{em} = 720-760 nm).

In the next step, we have studied the temperature sensing capabilities of ND_{SiV}-polymer. In bulk diamond with SiV, a ZPL shift of about 0.0124 nm per 1 K was demonstrated[10]. In the same work, a change in the intensity of SiV fluorescence in NDs with a size of 200 nm was shown. NDs with NV were used for intracellular thermometry[28], but such experiments require microwave field while SiV offers pure optical measurements. However, NDs with SiV have not been tested yet for thermometry by ZPL shift measurements. Herein, we analyzed spectra of 12 ND-SiV spots in water at temperatures ranging from 25°C to 37.5°C with a step of 2.5°C. The experiments were performed at a customized confocal microscope upgraded with a cell incubator (OkoLab, H301-MINI) with temperature stabilization for 25-40°C with an accuracy of 0.1°C. At 25°C (Figure 4a) the ND-SiV spectra revealed varying ZPL peak positions and widths (Figure 4b and 4c, Figure S15a and S15b), which could be a result of the crystal strain due to additional diamond defects, varying NDs shapes and morphologies, arbitrary positions of the SiV centers, the number of the SiV centers per nanocrystal, and the number of NDs in one spot[29]. For a significant temperature increase from 25°C to 37.5°C, we observed the red-shift of SiV ZPL for each spot (Figure 4b, Figure S15a). However, for some spots at intermediate temperatures between 25°C and 37.5°C, a deviation of ZPL shift was observed (Figure S15a). Particularly, only five out of 12 ND-SiV spots that had a ZPL peak position below 738.20 nm and a FWHM smaller than 4.6 nm showed a linear red-shift of ZPL $\Delta\lambda/\Delta T$ = ~0.011 - 0.013 nm/K (deviation ≤ 8.42%) for each measured

temperatures (Figure 4b). The remaining seven spots with ZPL peaks above 738.20 nm and FWHM larger than 4.6 nm revealed a strong deviation of the ZPL shift for small temperature steps (Figure S15a). Such behavior relates to crystal strain, which varies from NDs to NDs due to different defects, SiV location, and NDs shapes. Based on the obtained results, we can conclude that thermometry with SiV in NDs is possible. Nevertheless, the precise detection of small temperature variations might be challenging to achieve, and the initial properties of the ND-SiV should be evaluated prior to thermometry measurements.

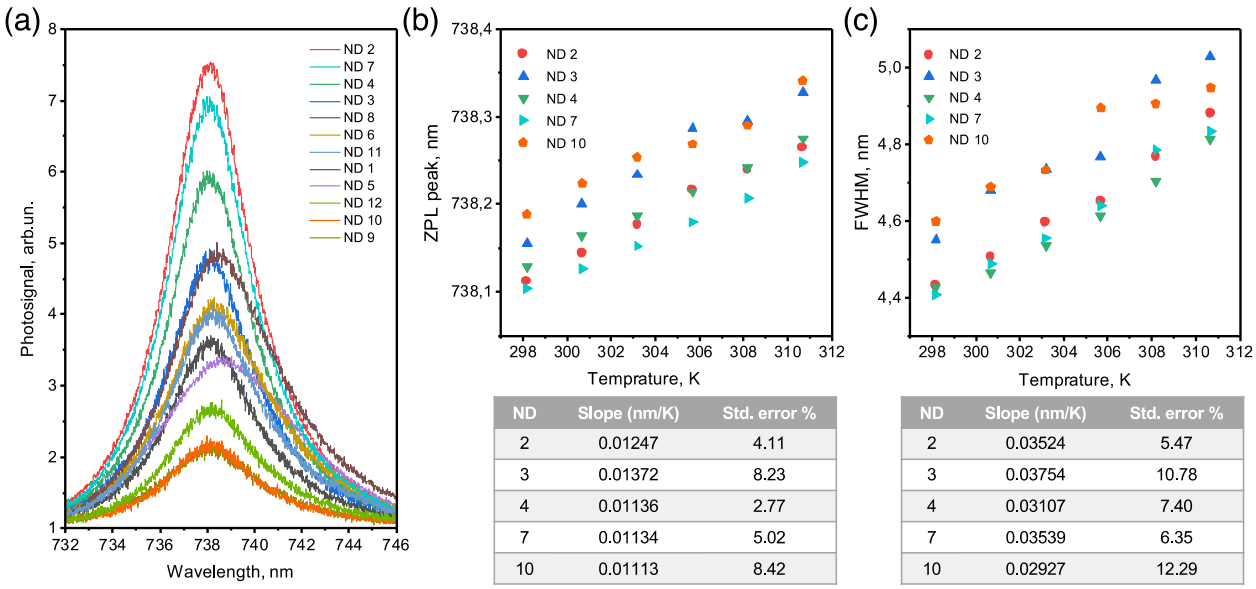

ND	Slope (nm/K)	Std. error %
2	0.01247	4.11
3	0.01372	8.23
4	0.01136	2.77
7	0.01134	5.02
10	0.01113	8.42

ND	Slope (nm/K)	Std. error %
2	0.03524	5.47
3	0.03754	10.78
4	0.03107	7.40
7	0.03539	6.35
10	0.02927	12.29

Figure 4. Thermal resonance of ND-SiV. (a) ZPL of 12 ND-SiV nanoparticles at 25°C. (b) Positions of ZPL peaks of five ND_{SiV} nanoparticles with a linear shift in the temperature range from 25°C to 37.5°C with low deviation. (c) FWHM of ZPL spectra for the five ND_{SiV} nanoparticles with a linear broadening in the temperature range from 25°C to 37.5°C with low deviation.

ND_{SiV}-polymer nanoparticles were tested for intracellular thermometry in fixed and living A549 cells, using fixed cells as a control to reduce the free motion of NDs compared with living cells

(living cell Figure 5a). We investigated the effect of the cellular environment on ND-SiV fluorescence since even low cellular autofluorescence can affect the detected SiV spectra and have an impact on temperature sensing. Within cells, the observed ND_{SiV}-polymer signals usually originate from ND clusters inside intracellular vesicles[30]. Unfortunately, all tested ND_{SiV}-polymer spots within cells had ZPL peaks above 738.2 nm at 25°C, which were not suitable for precise temperature sensing in the cells. Nevertheless, all the measuremd spots revealed thermo-resonance with red-shifts of the peak positions of their ZPL (Figure S17). One of the measured spots of ND_{SiV}-polymer in living cells demonstrated a red-shift of about ~0.06218 nm (average for seven measurements) (Figure 5b, Figure S17) after increasing the temperature from 25°C to 37°C. The live-cell thermometry with ND-SiV requires not only sensing but also a possibility to track the NDs. As a preliminary attempt, we have tracked 135 single ND_{SiV}-polymer spots within living HeLa cells for 90 min each with refocusing intervals of 40 s. The representative trajectory of one ND_{SiV} spot is shown in Figure 5c. The tracking measurements were accomplished by the fluorescence intensities of ND_{SiV}-polymer during the tracking experiments. The fluorescence intensities of tracked ND_{SiV}-polymer remained relatively stable (Figure 5c) with low fluctuations in the fluorescence intensity. These fluctuations could be attributed to the fast diffusion from the focal point of the objective or to rotational movement induced by different excitation efficiencies leading to changes in fluorescence intensity during tracking. The additional tracked intracellular NDs with representative trajectories and intensities are depicted in Figure S18a and S18b, and the presence of SiV centers was proven by spectral measurements (Figure S18c). In general, we did not observe a significant decrease in the fluorescence intensities indicating that ND_{SiV}-polymer allow long-term cellular tracking studies.

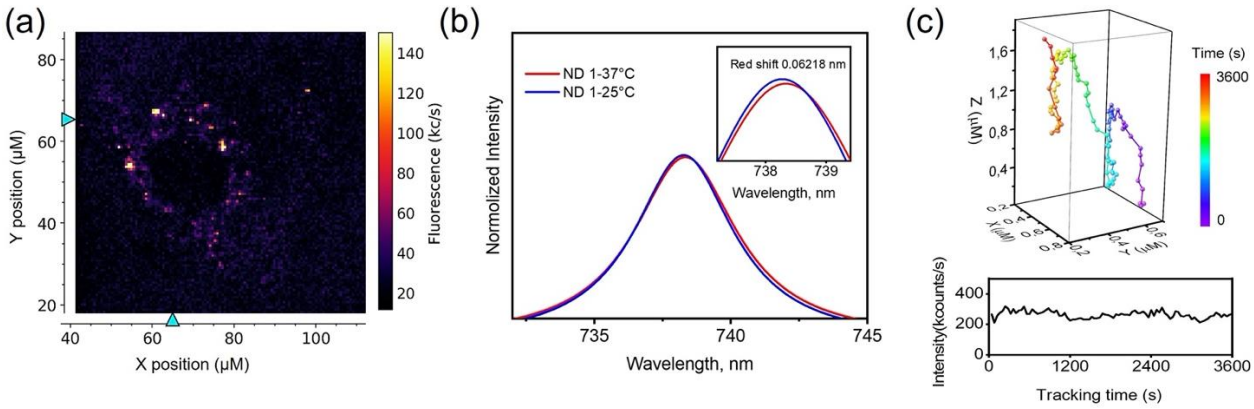

Figure 5. ND_{SiV}-polymer for living cell thermometry and intracellular tracking. (a) Custom-built confocal image of living A549 cell with uptaken ND_{SiV}-polymer nanoparticles. (b) The position of ZPL peaks of ND_{SiV}-polymer at 25°C and 37°C. (c) The trajectory of NDs_{SiV}-polymer tracked in intracellular space.

We have reported live-cell dual-color imaging, temperature sensing, and tracking applications of NDs containing only SiV centers and no other color centers produced by the improved metal-catalyst-free HPHT method. In this way, NIR emitters were obtained with a single sharp emission signal. These ND-SiV were coated with a protein-derived biopolymer that imparts colloidal stability in water, buffer, as well as in cell media. NIR fluorescence, sharp ZPL, and high fluorescence stability were key characteristics of these nanoemitters qualifying them for living cell imaging and tracking. For the first time, HPHT ND-SiV were observed in dual-color imaging and tracking experiments for up to 90 min inside living cells without photobleaching. Thermometry was investigated for the first time with small ND-SiV in water and cells, and a new singularity of ZPL shift with heat was found. We envision that ND-SiV represent a powerful tool for intracellular imaging[31], thermometry[10], and tracking[32], which renders them attractive for biological studies with intracellular real-time all-optical temperature sensing. However, thermometry with ND-SiV still requires deep and multidimensional investigations.

Since NDs can be also used for drug delivery,[23] a combination of all demonstrated properties of the ND-SiV system paves the way towards theranostic applications.

Supporting Information. The Supporting Information is available free of charge on the ACS Publications website at XXX

AUTHOR INFORMATION

Corresponding Author

*anna.ermakova@mpip-mainz.mpg.de, *fedor.jelezko@uni-ulm.de, *weil@mpip-mainz.mpg.de

Present Addresses

†If an author's address is different than the one given in the affiliation line, this information may be included here.

Author Contributions

W. Liu, A. Ermakova, and T. Weil initiated the draft. T. Weil and F. Jelezko acquired funding and initiated the project, supervised the students and revised the main manuscript. V. N. Agafonov, V. A. Davydov and R. Uzbekov contributed to the HPHT ND-SiV synthesis and raw material characterization. H. Qi and U. Kaiser contributed to the HRTEM characterization. W. Liu and M. N. A. Alam contributed to the ND-SiV acid treatment, ND_{SiV}-polymer preparation and characterization, cell experiments, bioimaging in CLSM microscopy (Zeiss 710), and intracellular spectral measurements in customized scanning confocal microscopy. A. Ermakova, Y. Liu and F. Jelezko contributed to the dual-color live-cell bioimaging, intracellular tracking, spectral measurements and are responsible for the photo physics. M. N. A. Alam and A. Ermakova contributed to the thermometry measurements by ND-SiV in water and cells in customized

scanning confocal microscopy. T. Lasser contributed writing the manuscript and interpreting experimental data. The manuscript was written through contributions of all authors. All authors have given approval to the final version of the manuscript.

Funding Sources

This work has been supported by the ERC Synergy grant no. 319130-BioQ. V. A. Davydov thanks the Russian Foundation for Basic Research (Grant No. 18-03-00936) for financial support. T.W. and F.J. acknowledge funding by the Deutsche Forschungsgemeinschaft (DFG, German Research Foundation) – Projektnummer 316249678 – SFB 1279 (C01, C04) and Projektnummer 318290668 – SPP 1923. F.J. acknowledge support by the Federal Ministry of Education and Research (BMBF) and VW foundation. H.Q. and U.K. gratefully acknowledge funding by the Deutsche Forschungsgemeinschaft (DFG, German Research Foundation) – Projektnummer 316249678 – SFB 1279 (Z01) and by the European Union's Horizon 2020 research and innovation programme under Grant Agreement No. 881603 (GrapheneCore3).

ACKNOWLEDGMENT

We thank Mrs. Katharina Maisenbacher (Max Planck Institute for Polymer Research, Germany) for the graph design. W. Liu acknowledges Dr. Todd Zapata (Max Planck Institute for Polymer Research, Germany) and Dr. Qiong Chen (Hunan Normal University, China) for very helpful scientific discussions.

ToC Figure: ND-SiV for cell imaging and intracellular thermosensing.

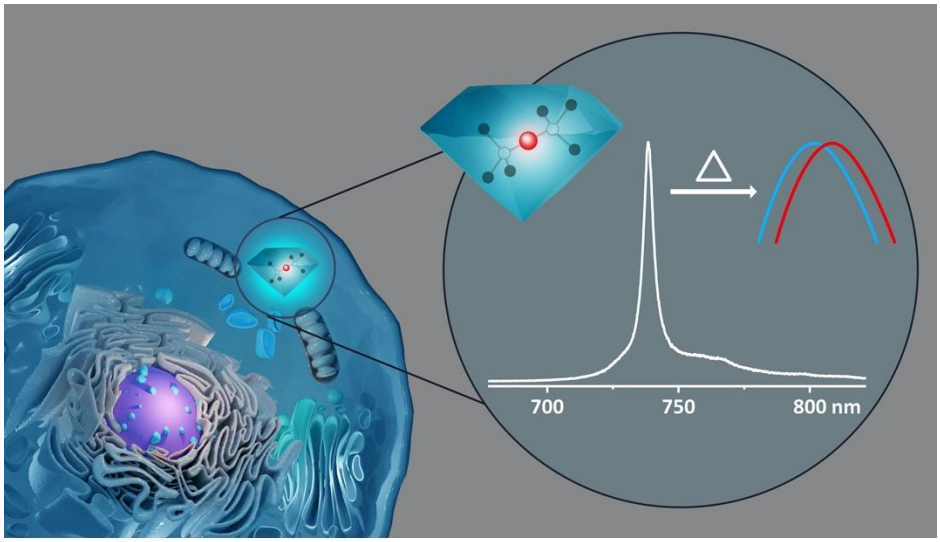

REFERENCES

[1] Yu, S.-J.; Kang, M.-W.; Chang, H.-C.; Chen, K.-M.; Yu, Y.-C., Bright Fluorescent Nanodiamonds: No Photobleaching and Low Cytotoxicity. *Journal of the American Chemical Society* **2005,** *127* (50), 17604–17605

[2] Tzeng, Y. K.; Faklaris, O.; Chang, B. M.; Kuo, Y.; Hsu, J. H.; Chang, H. C., Superresolution Imaging of Albumin‐Conjugated Fluorescent Nanodiamonds in Cells by Stimulated Emission Depletion. *Angewandte Chemie International Edition* **2011,** *50* (10), 2262-2265.

[3] Hsiao, W. W.-W.; Hui, Y. Y.; Tsai, P.-C.; Chang, H.-C., Fluorescent Nanodiamond: A Versatile Tool for Long-Term Cell Tracking, Super-Resolution Imaging, and Nanoscale Temperature Sensing. *Accounts of Chemical Research* **2016,** *49* (3), 400-407.

[4] Ermakova, A.; Pramanik, G.; Cai, J.-M.; Algara-Siller, G.; Kaiser, U.; Weil, T.; Tzeng, Y.-K.; Chang, H.; McGuinness, L.; Plenio, M., Detection of a few metallo-protein molecules using color centers in nanodiamonds. *Nano letters* **2013,** *13* (7), 3305-3309.

[5] Chang, Y.-R.; Lee, H.-Y.; Chen, K.; Chang, C.-C.; Tsai, D.-S.; Fu, C.-C.; Lim, T.-S.; Tzeng, Y.-K.; Fang, C.-Y.; Han, C.-C.; Chang, H.-C.; Fann, W., Mass production and dynamic imaging of fluorescent nanodiamonds. *Nature Nanotechnology* **2008**, *3*, 284-288.

[6] Doherty, M. W.; Manson, N. B.; Delaney, P.; Jelezko, F.; Wrachtrup, J.; Hollenberg, L. C., The nitrogen-vacancy colour center in diamond. *Physics Reports* **2013,** *528* (1), 1-45.

[7] Vlasov, I. I.; Shiryaev, A. A.; Rendler, T.; Steinert, S.; Lee, S.-Y.; Antonov, D.; Vörös, M.; Jelezko, F.; Fisenko, A. V.; Semjonova, L. F.; Biskupek, J.; Kaiser, U.; Lebedev, O. I.; Sildos, I.; Hemmer, P. R.; Konov, V. I.; Gali, A.; Wrachtrup, J., Molecular-sized fluorescent nanodiamonds. *Nature Nanotechnology* **2013,** *9*, 54-58.

[8] Weissleder, R., A clearer vision for in vivo imaging. *Nature Biotechnology* **2001,** *19*, 316-317.

[9] Sajedi, S.; Sabet, H.; Choi Hak, S., Intraoperative biophotonic imaging systems for image-guided interventions. *Nanophotonics* **2018,** *8* (1), 99-116.

[10] Nguyen, C. T.; Evans, R. E.; Sipahigil, A.; Bhaskar, M. K.; Sukachev, D. D.; Agafonov, V. N.; Davydov, V. A.; Kulikova, L. F.; Jelezko, F.; Lukin, M. D., All-optical nanoscale thermometry with silicon-vacancy centers in diamond. *Applied Physics Letters* **2018,** *112* (20), 203102.

[11] Grudinkin, S. A.; Feoktistov, N. A.; Baranov, M. A.; Smirnov, A. N.; Davydov, V. Y.; Golubev, V. G., Low-strain heteroepitaxial nanodiamonds: fabrication and photoluminescence of silicon-vacancy colour centers. *Nanotechnology* **2016,** *27* (39), 395606.

[12] Vlasov, I. I.; Barnard, A. S.; Ralchenko, V. G.; Lebedev, O. I.; Kanzyuba, M. V.; Saveliev, A. V.; Konov, V. I.; Goovaerts, E., Nanodiamond Photoemitters Based on Strong Narrow-Band Luminescence from Silicon-Vacancy Defects. *Advanced Materials* **2009,** *21* (7), 808-812.

[13] Shenderova, O. A.; Shames, A. I.; Nunn, N. A.; Torelli, M. D.; Vlasov, I.; Zaitsev, A., Review Article: Synthesis, properties, and applications of fluorescent diamond particles. *Journal of Vacuum Science & Technology B* **2019,** *37* (3), 030802.

[14] Davydov, V. A.; Rakhmanina, A. V.; Agafonov, V.; Narymbetov, B.; Boudou, J. P.; Szwarc, H., Conversion of polycyclic aromatic hydrocarbons to graphite and diamond at high pressures. *Carbon* **2004,** *42* (2), 261-269.

[15] Davydov, V. A.; Rakhmanina, A. V.; Lyapin, S. G.; Ilichev, I. D.; Boldyrev, K. N.; Shiryaev, A. A.; Agafonov, V. N., Production of nano- and microdiamonds with Si-V and N-V luminescent centers at high pressures in systems based on mixtures of hydrocarbon and fluorocarbon compounds. *JETP Letters* **2014,** *99* (10), 585-589.

[16] Davydov, V. A.; Agafonov, V.; Khabashesku, V. N., Comparative Study of Condensation Routes for Formation of Nano- and Microsized Carbon Forms in Hydrocarbon, Fluorocarbon, and Fluoro-Hydrocarbon Systems at High Pressures and Temperatures. *The Journal of Physical Chemistry C* **2016,** *120* (51), 29498-29509.

[17] Choi, S.; Leong, V.; Davydov, V. A.; Agafonov, V. N.; Cheong, M. W. O.; Kalashnikov, D. A.; Krivitsky, L. A., Varying temperature and silicon content in nanodiamond growth: effects on silicon-vacancy centers. *Scientific Reports* **2018,** *8* (1), 3792.

[18] Davydov, V. A.; Rakhmanina, A. V.; Agafonov, V.; Khabashesku, V. N., On the nature of simultaneous formation of nano- and micron-size diamond fractions under pressure–temperature-induced transformations of binary mixtures of hydrocarbon and fluorocarbon compounds. *Carbon* **2015,** *90*, 231-233.

[19] Nagl, A.; Hemelaar, S. R.; Schirhagl, R., Improving surface and defect center chemistry of fluorescent nanodiamonds for imaging purposes—a review. *Analytical and Bioanalytical Chemistry* **2015,** *407* (25), 7521-7536.

[20] Osswald, S.; Yushin, G.; Mochalin, V.; Kucheyev, S. O.; Gogotsi, Y., Control of sp2/sp3 Carbon Ratio and Surface Chemistry of Nanodiamond Powders by Selective Oxidation in Air. *Journal of the American Chemical Society* **2006,** *128* (35), 11635-11642.

[21] Koynov, K.; Butt, H.-J., Fluorescence correlation spectroscopy in colloid and interface science. *Current Opinion in Colloid & Interface Science* **2012,** *17* (6), 377-387.

[22] Schaeffel, D.; Yordanov, S.; Staff, R. H.; Kreyes, A.; Zhao, Y.; Schmidt, M.; Landfester, K.; Hofkens, J.; Butt, H.-J.; Crespy, D.; Koynov, K., Fluorescence Correlation Spectroscopy in Dilute Polymer Solutions: Effects of Molar Mass Dispersity and the Type of Fluorescent Labeling. *ACS Macro Letters* **2015,** *4* (2), 171-176.

[23] Wu, Y.; Ermakova, A.; Liu, W.; Pramanik, G.; Vu, T. M.; Kurz, A.; McGuinness, L.; Naydenov, B.; Hafner, S.; Reuter, R.; Wrachtrup, J.; Isoya, J.; Förtsch, C.; Barth, H.; Simmet, T.;

Jelezko, F.; Weil, T., Programmable Biopolymers for Advancing Biomedical Applications of Fluorescent Nanodiamonds. *Advanced Functional Materials* **2015,** *25* (42), 6576-6585.

[24] Wu, Y.; Eisele, K.; Doroshenko, M.; Algara-Siller, G.; Kaiser, U.; Koynov, K.; Weil, T., A Quantum Dot Photoswitch for DNA Detection, Gene Transfection, and Live-Cell Imaging. *Small* **2012,** *8* (22), 3465-3475

[25] Zhang, T.; Neumann, A.; Lindlau, J.; Wu, Y.; Pramanik, G.; Naydenov, B.; Jelezko, F.; Schüder, F.; Huber, S.; Huber, M.; Stehr, F.; Högele, A.; Weil, T.; Liedl, T., DNA-Based Self-Assembly of Fluorescent Nanodiamonds. *Journal of the American Chemical Society* **2015,** *137* (31), 9776-9779.

[26] Merson, T. D.; Castelletto, S.; Aharonovich, I.; Turbic, A.; Kilpatrick, T. J.; Turnley, A. M., Nanodiamonds with silicon vacancy defects for nontoxic photostable fluorescent labeling of neural precursor cells. *Optics Letters* **2013,** *38* (20), 4170-4173.

[27] Neu, E.; Agio, M.; Becher, C., Photophysics of single silicon vacancy centers in diamond: implications for single photon emission. *Optics Express* **2012,** *20* (18), 19956-19971.

[28] Wu Y.; Alam, M. N. A.; Balasubramanian, P.; Ermakova, A.; Fischer, S.; Barth, H.; Wagner, M.; Raabe, M.; Jelezko, F.; Weil, T., Nanodiamond Theranostic for Light-Controlled Intracellular Heating and Nanoscale Temperature Sensing, Nano Letters **2021**, 21 (9), 3780–3788

[29] Lindner, S.; Bommer, A.; Muzha, A.; Krueger, A.; Gines, L.; Mandal, S.; Williams, O.; Londero, E.; Gali, A.; Becher, C., Strongly inhomogeneous distribution of spectral properties of silicon-vacancy color centers in nanodiamonds. *New Jouranal of Physics* **2018**, *20*, 115002

[30] Liu, W.; Naydenov, B.; Chakrabortty, S.; Wuensch, B.; Hübner, K.; Ritz, S.; Cölfen, H.; Barth, H.; Koynov, K.; Qi, H.; Leiter, R.; Reuter, R.; Wrachtrup, J.; Boldt, F.; Scheuer, J.; Kaiser, U.; Sison, M.; Lasser, T.; Tinnefeld, P.; Jelezko, F.; Walther, P.; Wu, Y.; Weil, T., Fluorescent Nanodiamond–Gold Hybrid Particles for Multimodal Optical and Electron Microscopy Cellular Imaging. *Nano Letters* **2016**, 16 (10), 6236–6244

[31] Han, S.; Raabe, M.; Hodgson, L.; Mantell, J.; Verkade, P.; Lasser, T.; Landfester, K.; Weil, T.; Lieberwirth, I., High-Contrast Imaging of Nanodiamonds in Cells by Energy Filtered and Correlative Light-Electron Microscopy: Toward a Quantitative Nanoparticle-Cell Analysis. *Nano Letters* **2019,** *19* (3), 2178-2185.

[32] Hui, Y. Y.; Hsiao, W. W-W.; Haziza, S.; Simonneau, M.; Treussart, F; Chang, H.-C., Single particle tracking of fluorescent nanodiamonds in cells and organisms. *Current Opinion in Solid State and Materials Science* **2017,** *21* (1), 35-42.